Numerical Studies on CFRP Strengthened Steel Columns under Transverse Impact

M. I. Alam [1], *S. Fawzia [1]

[1] *School of Civil Engineering and Built Environment, Faculty of Science and Engineering, Queensland University of Technology, 2 George Street, Brisbane, QLD 4000, Australia*

(*Corresponding Author: sabrina.fawzia@qut.edu.au

Tel: 61 7 3138 1012 Fax: 61 7 3138 1170)

Abstract

Strengthening of metallic structures using carbon fibre reinforced polymer (CFRP) has become a smart strengthening option over the conventional strengthening method. Transverse impact loading due to accidental vehicular collision can lead to the failure of existing steel hollow tubular columns. However, knowledge is very limited on the behaviour of CFRP strengthened steel members under dynamic impact loading condition. This paper deals with the numerical simulation of CFRP strengthened square hollow section (SHS) steel columns under transverse impact loading to predict the behaviour and failure modes. The transverse impact loading is simulated using finite element (FE) analysis based on numerical approach. The accuracy of the FE modelling is ensured by comparing the predicted results with available experimental tests. The effects of impact velocity, impact mass, support condition, axial loading and CFRP thickness are examined through detail parametric study. The impact simulation results indicate that the strengthening technique shows an improved impact resistance capacity by reducing lateral displacement of the strengthened column about 58% compared to the bare steel column. Axial loading plays an important role on the failure behaviour of tubular column.

Keywords: CFRP; Square hollow section (SHS); Steel column; Numerical simulation; Transverse impact.

Nomenclature

COV	Coefficient of variance
E_p	Plastic modulus of steel
E_s	Elastic modulus of steel
E_{CFRP}	Tensile modulus of CFRP lamina in fibre direction
E_{GFRP}	Tensile modulus of GFRP lamina in fibre direction
F_y	Yield stress of steel
M	Impactor mass
P	Applied static axial load
P_{FE}	Ultimate axial load from FE analysis
P_{test}	Ultimate axial load from experimental test
U_{FE}	Axial shortening at ultimate axial load from FE analysis
U_{Test}	Axial shortening at ultimate axial load from experimental test
V	Initial impact velocity
X_{CFRP}	Tensile strength of CFRP lamina
X_{GFRP}	Tensile strength of GFRP lamina
ν	Poission's ratio of steel
$\varepsilon_{t(CFRP)}$	Failure tensile strain of CFRP lamina
$\varepsilon_{c(CFRP)}$	Failure compressive strain of CFRP lamina
$\varepsilon_{t(GFRP)}$	Failure tensile strain of GFRP lamina
$\varepsilon_{c(GFRP)}$	Failure compressive strain of GFRP lamina
ρ_s	Density of steel
ρ_{CFRP}	Density of dry CFRP fabric
ρ_{GFRP}	Density of dry GFRP fabric

1. Introduction

Application of carbon fibre reinforced polymer (CFRP) to strengthen/retrofit civil infrastructures has gained strong attraction to the researchers due to its unique high strength to weight ratio property. The successful utilisation of CFRP composites in reinforced concrete structures [1, 2] has attracted considerable interest on using such technique in metallic civil infrastructure. Recently a number of experimental tests and numerical analyses have been conducted to evaluate the performance of CFRP strengthened steel structures. Since last decade, extensive studies have been conducted to understand the static behaviour of CFRP strengthened steel members subjected to static loading and the findings are well documented in several research articles [3-11].

A good number of research works have been carried out to investigate the axial capacity of CFRP strengthened steel tubular members due to static loading. Shaat and Fam [12-14] explored the performance enhancement of CFRP strengthened square hollow section (SHS) short and long steel columns. Another study was conducted by Fawzia et al. [15] to evaluate the effectiveness of high modulus CFRP sheets for strengthening of circular hollow sections

(CHS) under static tensile loading. A significant improvement of compressive strength of CFRP strengthened CHS and SHS steel stub columns was noticed from the experimental tests [7, 16].

Hollow tubular members have been used extensively in many mission critical infrastructures as a compressive member where transverse impact force most likely to occur due to ships or vehicular collisions. Several past researches and statistic data have shown that vehicular collision is one of the main causes of structural failure [17-19]. The previous researches [20, 21] clearly indicate that the hollow tubular members are prone to transverse impact loading (e.g. vehicular impact, ship impact). These steel tubular members might experience severe damage or failure due to imposed transverse force from the moving vehicles. In recent years, very few work have found in the literature to investigate the axial and tensile impact effects on the CFRP strengthened steel tubes and plates. Experimental tests have been performed to evaluate the axial capacity of CFRP strengthened steel and aluminium hollow square tubes under axial impact loadings [22-24]. The results have shown a great potential of CFRP strengthening system by enhancing the energy absorption capacity and improving the crashworthiness parameters. Recently, Al-Zubaidy et al. [25-27] carried out experiments and numerical investigation on the responses of CFRP-steel plate joints under tensile impact loads. Mechanical properties of CFRP and adhesive were obtained under dynamic tensile loading and empirical formulas were derived to account the strain-rate effect in CFRP and epoxy adhesive. However, tubular columns, utility poles or offshore structures are often experienced transverse impact forces from vehicular/ship accidents rather than the axial impact loading. The transverse impact force on the columns is most common type of impact loading and suitable strengthening technique is required to minimise the impact damage. The above literature clearly indicates that the behaviour of CFRP strengthened steel columns under transverse impact loading has not been addressed previously by others. The aim of this research is to evaluate the performance of CFRP strengthening/retrofitting of existing hollow steel members subjected to transverse impact loading.

This study focuses on the numerical investigation of the CFRP strengthened SHS steel columns subjected to transverse impact loading. Numerical modelling and analysis have been performed using ABAQUS [28] and validated using existing experimental results in literature [12, 20]. Later, transverse impact simulation is carried out at the mid-height distance of strengthened and bare steel columns. A detail parametric study is conducted to evaluate the

effects of initial impact velocity, impactor mass, support conditions, axial loading, and CFRP reinforcing thickness on the behaviour of CFRP strengthened columns subjected to transverse impact loading.

2. Finite element modelling and validation

Initially the impact simulation process is validated followed by the model validation and parametric studies using ABAQUS software package. As there is insufficient experimental data and results on the behaviour of CFRP strengthened columns due to transverse impact loading, thus the validation of numerical modelling and dynamic analyses are conducted in two step process. In first step, the dynamic impact simulation process is validated by developing finite element (FE) model of a CHS bare steel tube and validating the results with drop mass impact tests [20]. Later in second step, CFRP strengthened SHS steel column is modelled and validated with the static compression test results conducted by Shaat and Fam [12]. Once the CFRP strengthened model is validated, then the dynamic impact simulation is performed by adopting the CHS steel tube impact simulation process to ensure reliable numerical analysis.

2.1 Validation of impact simulation process

The present numerical model is built in the ABAQUS/Explicit environment to validate Zeinoddini et al. [20] experimental impact tests. The FE model is built with four parts representing the CHS steel tube, the drop mass, transverse spring, and longitudinal spring. The steel tube is modelled with 4-node shell element (S4R) with reduced integration and hourglass control. This type of element is recommended for large strain or rotational analysis [28]. The isotropic classic metal plasticity model available in ABAQUS/Explicit has been used to simulate the elasto-plastic behaviour of CHS tube. Modulus of elasticity, yield stress, and density of steel tube are chosen form the Zeinoddini et al. [20] as 200 GPa, 500 MPa and 7850 kg/m^3 respectively. No strain rate effect has been taken into account as high tensile steel has low sensitivity to strain rates [29]. The drop hammer is modelled using 8-node linear brick element with reduced integration and hourglass control (C3D8R). The density of the hammer is specified for a mass of 25.45 kg as used in the experiment.

The supports of axially loaded steel tube are assigned with the boundary conditions in horizontal, vertical and axial directions. The right end of CHS specimen is fixed by introducing a reference point at the centre of the hollow section (right end). The boundary conditions are applied to the reference point to restrain its movement in all degrees of freedom while all the peripheral nodes of CHS are constrained with the reference point by using multi point constraints (MPC) available in ABAQUS [28]. A longitudinal spring is modelled at the left end of the specimen to apply axial loading as mentioned in the experiment [20]. One end of spring is attached to a reference point which is constrained with the circumference of left end of steel tube using kinematic coupling tie (Fig. 1). The other end of the axial spring is restrained in axial direction of the tube to apply axial loading. A transverse spring with minor stiffness is also modelled to consider friction force developed in the vertical guide during impact tests.

The simulation of axially loaded CHS tube subjected to transverse impact loading is two-step process. In the first step of analysis, the axial load is applied in quasi-static manner during the lower natural period of the structure. The smooth step amplitude available in ABAQUS [28] has been used to apply axial displacement on the left end of longitudinal spring. The stiffness and applied displacement of the spring are adjusted to induce 50% and 70% of the steel tube squash load [20] at the right end of the spring (Fig. 1). After the end of quasi-static analysis step the impact loading step is started and a contact interaction is developed between the steel tube outer surface and the sharp edge indentor (impact hammer). The surface-to-surface contact option available in ABAQUS is deployed to model load transfer mechanism between the impactor and the CHS tube. The indentor outer surface and the steel outer surface are defined as master and slave surfaces. The surface-to-surface approach has been chosen due to more realistic stress distribution compared to node-to-surface contact algorithm [28]. Penalty and hard contact methods are adopted to define the tangential and normal behaviour of contact interaction with the value of 0.47 coefficient of friction [30]. The predefined field option in ABAQUS/Explicit is used to apply the initial velocity of 7 m/s to the indentor to cause transverse impact on the steel tube.

The comparison of failure modes of Zeinoddini et al. [20] and present numerical simulation is shown in Fig. 2. It is observed that the current FE simulation can predict the failure modes of 0%, 50%, and 70% axially loaded steel tube under transverse impact loading reasonably. The CHS tube with 70% axial loading has shown global failure behaviour with large lateral and

axial displacement as depicted in the earlier experimental tests and numerical simulations [20, 30, 31]. Fig. 3(a) shows good agreement of transverse impact force-time curves between the tests and FE analyses under 0%, 50% and 70% of compressive loading. Furthermore, the well matched lateral displacement-time curves in Fig. 3(b) ensure the reliability of present numerical simulation process under combined axial and impact loading.

2.2 Numerical simulation of CFRP strengthened slender column

2.2.1 Finite Element Modelling Approach

CFRP strengthened SHS steel column has been modelled and validated against axial compressive loading using available experimental results [12]. The detail of experiment set-up and procedure can be found in Shaat and Fam [12]. Three-dimensional finite element models of bare steel column (control) and 2 strengthened columns with sectional dimension of 89 mm × 89 mm × 3.2 mm and length of 2380 mm are developed in ABAQUS. The FE modelling involves creating of three different part instances: SHS steel column, end plates (steel cap), and composite laminates as shown in Fig. 4(a). The control specimen is modelled using the 4-node shell element (S4R) with reduced integration and hourglass control whereas the end steel caps are model by 8-node linear solid element with reduced integration and hourglass control (C3D8R). Composite lay-up technique is deployed to model the composite laminates. Composite laminates are the orientation of CFRP (three layers two sides and three layers four sides) and GFRP (one layer two sides and one layer four sides) layers in the longitudinal direction of column as described in the experiment [12]. The conventional shell elements (S4R) are also used to model composite laminates and no adhesive element is modelled as each lamina is prepared by wet lay up of dry fabric with resin. The thickness of CFRP and GFRP lamina are assigned as 0.54 mm and 1.46 mm respectively to ensure identical with the measured thickness during experiment [12]. Suitable mesh sizes with relatively fine mesh density at the corner regions are selected as shown in Fig. 4(a). The mesh size of composite laminates is same as the flat portion of the steel column to constrain each other. The solid end plates at both ends of column are tied together with the matching nodes (Fig. 4(a)). Tie constrains are utilised to establish the connection between the steel surface and composite laminates of strengthened columns.

2.2.2 Boundary conditions and load application

The support conditions are applied along the middle line of the end steel plates to keep it consistent with the experiment. The translational degrees of freedom of loading end plate are constrained in the transverse two directions and released in the loading direction (longitudinal direction). The other end plate of the column is constrained in all three translation degrees of freedom whereas all rotational degrees of freedom of both ends of the column are released to achieve the hinge support condition. The validation of bare and strengthened SHS columns under axial loading is a two-step analysis process. Initially the buckling analysis is conducted to predict the buckling mode of columns with linear material properties followed by a non-linear static analysis using modified RIKS method [28]. The first buckling mode of bare steel column is shown in Fig. 4(b) after the end of buckling analysis. The measured geometric imperfections of slender columns [12] are considered in the non-linear static analysis to initiate the global buckling failure at the mid-height regions of columns as observed during experiment [12]. The axial load is applied incrementally at the centre of the loading end plate using displacement control approach.

2.2.3 Material models

The stress-strain relation of steel column is defined by the bi-linear model using *PLASTIC option in ABAQUS [28]. The plasticity modulus of the curve is assumed 50% of elastic modulus of steel [14, 32] (Fig. 5). The modulus of elasticity and yield stress are same as mentioned in Shaat and Fam [12]. The material properties of both CFRP and GFRP lamina are obtained from the coupon test results conducted by Shaat [33]. However, the densities are collected from the material testing data of CFRP and GFRP manufacturers. The CFRP laminates are modelled using lamina type elastic material and well known “Hashin” failure criteria [34, 35] is adopted to model the failure behaviour. This damage model available in ABAQUS [28] is suitable to predict the damage and failure of elastic-brittle materials and successfully adopted in other researches [27, 36]. The damage evaluation is described as degradation of material stiffness and removal of elements once failure criteria are achieved. The failure tensile strains of CFRP and GFRP are adopted as 0.22% and 0.2% respectively [33]. The failure compressive strains are chosen as 60% of tensile strain as suggested in Shaat and Fam [37]. All the material properties use for the current FE analyses are listed in Table 1.

2.2.4 Validation of numerical model

The results obtained from the FE analysis are compared with the Shaat and Fam [12] experiments to validate the control and strengthened columns. The measured and predicted ultimate failure loads and axial displacements at failure are compared in Table 2. A good agreement is observed between experimental test and FE models as the mean ratio and COV of ultimate load are 0.98 and 0.036 respectively. A good agreement is also noticed for axial shortening at failure load as the mean ratio and COV are 0.99 and 0.031 respectively. Fig. 6 shows the comparison of axial load-displacement curves and failure behaviour of test and FE columns. Good matching between load-displacement curves of all three types of column is noticed. Furthermore, failure mode of FE analysis model is similar with the tested strengthened column (Fig. 6(b)). The column fails around the mid-height with compression face inward buckling and side faces outer buckling as observed in the experiment [12]. However, no CFRP deboning/delamination is found as no adhesive element is modelled between the composite lamina and steel surface.

3. Impact Simulation of CFRP strengthened column

Currently there is no available experimental data on the CFRP strengthened columns under transverse impact loading. Therefore, the validated bare steel and strengthened columns are utilised to conduct explicit dynamic analysis under transverse impact loading to investigate the strengthening effects. The impact simulation process discussed in section 2 is adopted to ensure reliable FE analysis. Fig. 7 shows the FE model of validated CFRP strengthened column with the impactor. The impactor is modelled as a rigid mass using 8-node brick element (C3D8R) with dimensions of 74 × 74 × 700 mm. The density of the impactor cube is calculated using its volume and expected mass. The initial impact velocity is generated at the outer surface of the impactor to create an impact collision at the mid height of the column. The surface to surface interaction method is employed to define the contact behaviour between the impactor front surface and column outer surface to propagate impact force from impactor to column. The effect of strain rate is introduced based on Cowper-Symonds power law with a multiplier factor of 40.4 s^{-1} and exponent of 5 as suggested for mild steel [29]. A number of studies have shown that the mechanical properties of carbon/epoxy and glass/epoxy composites are almost strain rate insensitive [38, 39]. Thus no strain rate effects are considered in CFRP and GFRP material models. In case of two sides strengthened column, the top and the bottom portions in Fig. 7(a) are strengthened and the other two sides are unstrengthened.

3.1 Impact simulation results

The results obtained from the FE analyses are presented in terms of impact force, lateral displacement, axial shortening, and failure modes. The initial impact velocity and impact mass are chosen as 7 m/s and 170 kg respectively. No axial load is applied and the support conditions are one end fixed and other end pined. Fig. 8 compares the impact force-time and impact force-lateral displacement responses of bare steel and CFRP strengthened columns. The impact force-time curves show that the initial peak forces of strengthened columns (two sides and four sides) are almost double compared to the control specimen (bare steel) model. However, the mean residual force of four sides strengthened column is more than the two sides strengthened column (Fig. 8(a)). Fig. 8(b) depicts the impact force-lateral displacement plots. The four sides strengthened column poses permanent lateral displacement of 37.57 mm whereas two sides strengthened and control columns have undergone large displacements of 96.70 mm and 89.76mm respectively. The same phenomena can be observed from the Fig. 9 and found that the four sides strengthened column performed well compared to two sides strengthened and control column. It is noticed from Fig. 8 and 9 that the two sides strengthened column experiences larger displacements (axial and lateral) compared to the control specimen. This can be explained from the high impact force and failure mode of two sides strengthened column. Two sides strengthened column gets high initial impact force due to CFRP strengthening at top and bottom sides only, however the unstrengthened two sides show excessive outward buckling due to larger impact force (Fig. 10). Outward buckling phenomena can lead the impact zone to weaker against impact loading causing large displacement. Fig. 10(c) demonstrates that the outward buckling of four sides strengthened column is not prominent compared to others, thus this type of strengthened column exhibits better performance in term of energy absorption capacity and buckling control against transverse impact loading.

3.2 Parametric Study

A range of parametric study is conducted to evaluate the effects of different parameters on the impact response of strengthened column.

3.2.1 Effects of impact velocity

The initial impact velocity of the impactor is varied from 4 m/s to 10 m/s and the impact mass is kept constant as 170 kg to investigate the velocity change effects on the responses of both

strengthened and control columns. Fig. 11 illustrates the lateral and axial displacement responses with respect to impact duration. Four sides strengthened column shows smaller displacement in both lateral and axial directions compared to two sides strengthened and control specimens. The displacement profiles of all columns under 4 m/s velocities are similar, however with the increase of velocity, two sides strengthened and control columns responses become straight. This occurs because under high impact velocity these columns unable to resist the impact force causing large displacements compared to four side strengthened column. In case of 10 m/s velocity the displacement of two sides strengthened columns in both axial and lateral directions are higher than the bare steel column. This may be occurred due to propagation of high stress concentration from strengthened regime (impact point) to unstrengthened regime which may result excessive outward buckling of unstrengthened zone as described in section 4.1. However, four sides strengthened column does not show excessive buckling from sides due to four sides CFRP wrapping and exhibits enhanced performance by minimising lateral and axial displacements 23% and 34.34% respectively compared to bare steel column under 10 m/s impact velocity. The effects of velocity changes on the impact force are displayed in Fig. 12. The initial peak impact forces are almost same in four sides and two sides strengthened columns compared to the bare steel column (Fig. 12(a)). However, initial peak forces are increasing steadily with the increase of the initial velocity. The mean residual force versus velocity change plots show different characteristics compared to the initial peak force graph. The four sides strengthened column poses increasing trend, whereas the other two column forces are decreasing with respect to velocity (Fig. 12(b)). The decreasing rate of two sides strengthened column is higher than the bare steel one. Therefore, it can be concluded that the columns with high residual forces performed better to minimise both axial and lateral displacements.

3.2.2 Effects of impact mass

The influences of impactor mass on the behaviour of impacted columns have shown in Fig. 13 and 14. The impact velocity is chosen as 7 m/s during the analyses period while impact mass is varied from 85 kg to 255 kg. The impactor mass has a noticeable effect on the axial shortening and the mid-height displacements of all three types of columns. The effect is more pronounced on two sides strengthened and control members than the four sides strengthened column (Fig. 13). On the other hand the effect of impact mass on the impact force is not significant compared to the velocity changes effect. Fig. 14(a) exhibits minor changes of

forces with the increase of impact mass. It is noticed that the lateral and axial displacements are almost similar for two sides strengthened and bare steel columns in high impact mass although the peak impact forces are almost same. The reason may be due to energy absorption capacity of two sides strengthened column is not significant compared to four sides strengthened column.

3.2.3 Effects of support conditions

The strengthened and bare steel columns are analysed in different boundary conditions (both end fixed, one end fixed and one end pinned, both end pinned) to observe their effects in impact loading events. The impact mass and velocity are set to 7 m/s and 170 kg. The influence is not prominent on the initial peak impact forces of all three types of column as initial peak impact forces are almost same in different support conditions as shown in Fig. 15. An obvious increase of mean residual forces has been observed when the column ends are constrained in all degrees of freedom. However, with the relaxing the rotational boundary condition the impact force durations are increased and indicated the decreasing of impact resistance of the columns (Fig. 15). Fig. 16 shows impact force-lateral displacement relationships under different support conditions. It is noticed that all three columns with fixed-fixed supports performed better than the other support conditions as they are capable of absorbing energy produced by the impactor with a minimum lateral displacements compared to fixed-pinned and pinned-pinned conditions. The four sides strengthened column shows greater impact resistance in all three supports conditions than the 2 side strengthened and bare steel columns as depicted in Fig. 16. It is found from Fig. 15 and 16 that after the initial peak force the impact force dramatically reduced to zero in most of the cases. The durations of zero forces are maximum for pinned-pinned condition and minimum for fixed-fixed condition. Furthermore, for bare steel member no zero forces observe in fixed-fixed and fixed-pinned conditions. Fig. 17 shows that the velocities of columns are more than the impactor velocity just after impact collisions occurs. The columns having the relaxed boundary conditions (pinned-pinned support) have got larger velocity than the fixed-fixed supported columns (Fig. 17) and short time separation between the columns and the impactors occurs. Thus it is clear from the Fig. 17 that impact force reduces to zero due to short time separation between the impactor and the columns just after the initial peak force. This phenomena of other types of column subjected to transverse impact load have been observed from experimental test [40].

3.2.4 Effects of axial loading

The effect of axial compressive loading is evaluated by applying axial loading in a separate analysis step as discussed in section 2.1. The axial loading is applied in terms of pressure force on the surface of end plate during the first natural periods of column models (Fig. 7(a)). Fig. 18 shows the uniform stress distribution of control column and axial loading profile of all three types of column at the end of loading phase. The impact velocity and mass are kept constant as 4 m/s and 170 kg respectively while the axial loads are varied from 0 to 70% of columns failure loads obtained from the Shaat and Fam experiment [12]. Table 3 provides a summary of axial loads applied in three different columns along with the failure status. The axial loading has remarkable effects on the failure behaviour of square hollow columns as illustrated in Fig. 19. The bare steel column fails while axial loading percentage increases to 50% of its ultimate failure load. However, two sides and four sides strengthened columns have shown stability under 50% of failure load and fail when axial loading percentage increases to 60% and 70% respectively of their failure loads. The failure modes of control and strengthened columns are local buckling failures at the impact zone. Excessive outward side buckling is observed in control and two sides strengthened columns, while four sides strengthened column experiences inward buckling at the side and outward buckling at the front of the column (Fig. 19). This change of local buckling behaviour of four sides strengthened columns can be occurred due to the strengthening effect. Fig. 20 presents lateral displacement-time histories of control and strengthened columns subjected to combine axial and impact loads. Larger lateral displacements of control and strengthened columns are observed with the increase of their axial loads. The columns pose large lateral displacements (Fig. 20) indicates buckling failure at the mid-height regimes due to excessive axial compressive loads.

3.2.5 Effects of CFRP thickness

It has been noticed that four sides strengthening technique is much effective in resisting impact loads by reducing axial and lateral displacements of column compared to two sides strengthening system. Thus, only four sides strengthening column is considered to investigate the effects of CFRP thickness by varying the CFRP reinforcement from 1 to 5 layers. Fig. 21 exhibits the impact force-lateral displacement plots of four sides strengthened columns with the increasing of CFRP reinforcement from 1 to 5 layers. Minor changes in initial peak forces have been noticed with the increase of CFRP thickness. The maximum and minimum impact

forces are 111.83 kN and 98.02 kN for 5 layers and 4 layers strengthened columns. However, the mean residual forces increase steadily from 45kN to 65kN with the increase of reinforcing layers. The influence of number of CFRP layers on the axial and lateral displacements is remarkable as shown in Fig. 22. By increasing the CFRP layers from 1 to 5, permanent lateral and axial displacements can be reduced to 58.5% and 76.3% respectively. In other way, the increase of CFRP layers contributes to the energy absorption capacity of columns by minimising the lateral displacements. The increased energy absorption capability of the CFRP strengthened metal beams with the increasing of CFRP layers have also been reported in experiments conducted under dynamic blast loading [41].

4. Conclusions

In this paper, FE models of externally bonded CFRP strengthened SHS steel columns with different wrapping schemes are developed and validated. The validated models are then utilised for a range of numerical simulation to investigate the effectiveness of CFRP strengthening system under transverse impact loading. This study confirms that the externally bonded CFRP composites are effective in enhancing impact resistance capacity of existing SHS steel columns. The core findings of this study can be summarised as follows:

- Four sides strengthening system is highly effective in buckling control of SHS steel columns by providing confinement from all four sides. A significant performance improvement of four sides strengthened columns under transverse impact loading is observed by minimising the lateral displacement at the impact zone about 58% compared to the bare steel column. However, two sides strengthen system is not effective due to large outward buckling tendency of unstrengthened sides. This tendency is also noticed in case of bare steel column. The previous studies [12, 37] of retrofitting SHS slender columns have indicated that both two sides and four sides strengthening systems are effective under static compressive loading. Thus, where transverse impact force is expecting to occur due to accidental actions, SHS steel columns should be retrofitted in all four sides to sustain both static compressive and imposed lateral impact loads.
- The effect of initial peak impact force on the displacement responses of strengthened columns is not prominent. However, the mean residual force plays a vital role as results have shown that the higher the mean residual forces higher the axial and lateral displacement control ability of strengthened columns.

- The initial impactor velocity is a key parameter as initial impact forces increase significantly with the increase of velocity from 4 m/s to 10 m/s. The increment rate is maximum for four sides strengthened columns compared to others. Moreover, four sides strengthened columns have shown enhance performance by keeping the axial and lateral displacements lower.
- Boundary conditions play important role on the behaviour of strengthened and bare steel columns. While initial peak impact forces are almost same for all three types of support conditions, the columns with fixed-fixed boundary conditions are more stable under transverse impact loading. The phenomena of dropping initial peak force to zero is explored and found that columns with weaker boundary conditions attain more initial velocity than the impactor and short term separation occurs between the columns and the impactors.
- Axial loading has an obvious effect on the failure mechanism of SHS columns. With the increase of axial loading lateral displacements of columns are increased, although the impact energy is constant. Four sides strengthening system is highly effective under combined axial and impact loading as 70% of its ultimate compressive load is needed to cause failure with large lateral displacement. However, bare steel column collapses while axial load increases to 50% of its ultimate compressive load. The above results confirm that strengthening of SHS columns with service loading is highly effective compared to unstrengthened column. Therefore, the current repair strategy can be implemented in the existing hollow tubular columns to minimise structural damage due to transverse impact loading.
- With the increase of CFRP thickness a gradual reduction of axial and lateral displacements are observed. This ensures the increased energy absorption ability of CFRP composites under transverse impact loading.

Acknowledgement

The authors would like to thank, Queensland University of Technology (QUT) for providing support to carry out the work reported in this paper. The authors also wish to thank the technical staff and IT staff in Science and Engineering Faculty at QUT for their assistance in carrying out this research.

References

[1] Teng JG, Chen J-F, Smith ST, Lam L. FRP - strengthened RC structures. West Sussex, UK: John Wiley & Sons, Ltd.; 2001.
[2] Rizkalla S, Hassan T, Hassan N. Design recommendations for the use of FRP for reinforcement and strengthening of concrete structures. Progress in Structural Engineering and Materials. 2003;5:16-28.
[3] Fawzia S. Evaluation of shear stress and slip relationship of composite lap joints. Composite Structures. 2013;100:548-53.
[4] Fawzia S, Zhao X-L, Al-Mahaidi R. Bond–slip models for double strap joints strengthened by CFRP. Composite Structures. 2010;92:2137-45.
[5] Fawzia S, Al-Mahaidi R, Zhao X-L. Experimental and finite element analysis of a double strap joint between steel plates and normal modulus CFRP. Composite structures. 2006;75:156-62.
[6] Fawzia S, Zhao X, Al-Mahaidi R, Rizkalla S. Bond characteristics between CFRP and steel plates in double strap joints. The International Journal of Advanced Steel Construction. 2005;1:17-27.
[7] Haedir J, Zhao X-L. Design of short CFRP-reinforced steel tubular columns. Journal of Constructional Steel Research. 2011;67:497-509.
[8] Colombi P, Poggi C. Strengthening of tensile steel members and bolted joints using adhesively bonded CFRP plates. Construction and Building Materials. 2006;20:22-33.
[9] Zhao X-L, Fernando D, Al-Mahaidi R. CFRP strengthened RHS subjected to transverse end bearing force. Engineering structures. 2006;28:1555-65.
[10] Kalavagunta S, Naganathan S, Bin Mustapha KN. Proposal for design rules of axially loaded CFRP strengthened cold formed lipped channel steel sections. Thin-Walled Structures. 2013;72:14-9.
[11] Gao X, Balendra T, Koh C. Buckling strength of slender circular tubular steel braces strengthened by CFRP. Engineering Structures. 2013;46:547-56.
[12] Shaat A, Fam A. Axial loading tests on short and long hollow structural steel columns retrofitted using carbon fibre reinforced polymers. Canadian Journal of Civil Engineering. 2006;33:458-70.
[13] Shaat A, Fam A. Slender Steel Columns Strengthened Using High-Modulus CFRP Plates for Buckling Control. Journal of Composites for Construction. 2009;13:2-12.
[14] Shaat A, Fam A. Finite element analysis of slender HSS columns strengthened with high modulus composites. Steel and Composite Structures. 2007;7:19-34.
[15] Fawzia S, Al-Mahaidi R, Zhao X, Rizkalla S. Strengthening of circular hollow steel tubular sections using high modulus CFRP sheets. Construction and Building Materials. 2007;21:839-45.
[16] Bambach M, Jama H, Elchalakani M. Axial capacity and design of thin-walled steel SHS strengthened with CFRP. Thin-Walled Structures. 2009;47:1112-21.
[17] Briaud J-L, E. Hunt B. Bridge Scour & the Structural Engineer. Structure Magazine, 2006. p. 59-61.
[18] Harik I, Shaaban A, Gesund H, Valli G, Wang S. United States Bridge Failures, 1951–1988. Journal of Performance of Constructed Facilities. 1990;4:272-7.
[19] Wardhana K, Hadipriono FC. Analysis of recent bridge failures in the United States. Journal of Performance of Constructed Facilities. 2003;17:144-50.
[20] Zeinoddini M, Parke G, Harding J. Axially pre-loaded steel tubes subjected to lateral impacts: an experimental study. International Journal of Impact Engineering. 2002;27:669-90.

[21] Bambach M, Jama H, Zhao X, Grzebieta R. Hollow and concrete filled steel hollow sections under transverse impact loads. Engineering structures. 2008;30:2859-70.
[22] Bambach MR, Elchalakani M, Zhao X. Composite steel–CFRP SHS tubes under axial impact. Composite Structures. 2009;87:282-92.
[23] Bambach M, Jama H, Elchalakani M. Static and dynamic axial crushing of spot-welded thin-walled composite steel–CFRP square tubes. International Journal of Impact Engineering. 2009;36:1083-94.
[24] Bambach M, Elchalakani M. Plastic mechanism analysis of steel SHS strengthened with CFRP under large axial deformation. Thin-walled structures. 2007;45:159-70.
[25] Al-Zubaidy HA, Zhao X-L, Al-Mahaidi R. Experimental evaluation of the dynamic bond strength between CFRP sheets and steel under direct tensile loads. International Journal of Adhesion and Adhesives. 2012;40:89–102.
[26] Al-Zubaidy H, Zhao X-L, Al-Mahaidi R. Mechanical characterisation of the dynamic tensile properties of CFRP sheet and adhesive at medium strain rates. Composite Structures. 2012;96:153–64.
[27] Al-Zubaidy H, Al-Mahaidi R, Zhao X-L. Finite element modelling of CFRP/steel double strap joints subjected to dynamic tensile loadings. Composite Structures. 2012;99:48-61.
[28] SIMULIA. ABAQUS analysis and theory manuals. Providence, RI, USA: SIMULIA, the Dassault Systèmes, Realistic Simulation; 2011.
[29] Jones N. Structural impact. UK: Cambridge University Press; 1997.
[30] Al-Thairy H, Wang Y. A numerical study of the behaviour and failure modes of axially compressed steel columns subjected to transverse impact. International Journal of Impact Engineering. 2011;38:732-44.
[31] Zeinoddini M, Harding J, Parke G. Axially pre-loaded steel tubes subjected to lateral impacts (a numerical simulation). International Journal of Impact Engineering. 2008;35:1267-79.
[32] Bruneau M, Uang C-M, Whittaker A. Ductile design of steel structures. New York: McGraw-Hill; 1998.
[33] Shaat A. Structural behaviour of steel columns and steel-concrete composite girders retrofitted using CFRP. PhD Thesis, Queen's University,Ontario, Canada, 2007.
[34] Hashin Z, Rotem A. A fatigue failure criterion for fiber reinforced materials. Journal of composite materials. 1973;7:448-64.
[35] Hashin Z. Failure criteria for unidirectional fiber composites. Journal of applied mechanics. 1980;47:329-34.
[36] Lesani M, Bahaari M, Shokrieh M. Numerical investigation of FRP-strengthened tubular T-joints under axial compressive loads. Composite Structures. 2013;100:71-8.
[37] Shaat A, Fam A. Fiber-Element Model for Slender HSS Columns Retrofitted with Bonded High-Modulus Composites. Journal of Structural Engineering. 2007;133:85-95.
[38] Jacob GC, Starbuck JM, Fellers JF, Simunovic S, Boeman RG. Strain rate effects on the mechanical properties of polymer composite materials. Journal of Applied Polymer Science. 2004;94:296-301.
[39] Kimura H, Itabashi M, Kawata K. Mechanical characterization of unidirectional CFRP thin strip and CFRP cables under quasi-static and dynamic tension. Advanced Composite Materials. 2001;10:177-87.
[40] Han L-H, Hou C-C, Zhao X-L, Rasmussen KJ. Behaviour of high-strength concrete filled steel tubes under transverse impact loading. Journal of Constructional Steel Research. 2014;92:25-39.
[41] Bambach MR, Zhao XL, Jama H. Energy absorbing characteristics of aluminium beams strengthened with CFRP subjected to transverse blast load. International Journal of Impact Engineering. 2010;37:37-49.

Figure Captions:

Fig. 1. (a) Simplified numerical modelling, (b) finite element meshing of axially loaded CHS steel tube.
Fig. 2. Comparison of failure modes between test and present FE analysis.
Fig. 3. (a) Impact force comparison at different axial loading, (b) mid height displacement comparison at zero axial loading.
Fig. 4. (a) Detail of FE Model, (b) first buckling mode
Fig. 5. Bi-linear steel material model.
Fig. 6. (a) Comparison of load-displacement response, (b) failure mode comparison (4 sides strengthened column).
Fig. 7. (a) Numerical model for impact analysis, (b) impactor model.
Fig. 8. (a) Impact force-time comparison, (b) impact force-lateral displacement comparison.
Fig. 9. (a) Lateral displacement-time curves, (b) axial displacement-time curves.
Fig. 10. Failure modes (a) control, (b) CFRP- 2 sides, (c) CFRP- 4 sides.
Fig. 11. Effect of impact velocity on the (a) lateral, (b) axial displacement of control and strengthened columns.
Fig. 12. Effect of impact velocity on the (a) initial peak impact force, (b) mean residual force of control and strengthened columns.
Fig. 13. Effect of impact mass on the (a) lateral, (b) axial displacement of control and strengthened columns.
Fig. 14. Effect of impact mass on the (a) initial peak impact force, (b) mean residual force of control and strengthened columns.
Fig. 15. Effect of support conditions on the impact force-time histories of (a) four sides strengthened, (b) two sides strengthened, (c) bare steel column.
Fig. 16. Effect of support conditions on the impact force-lateral displacement responses of (a) four sides strengthened, (b) two sides strengthened, (c) bare steel column.
Fig. 17. Velocity-time curves of impactor and columns at mid-height under (a) fixed-fixed, (b) pinned-pinned support conditions.
Fig. 18. (a) Stress distribution at the end of quasi-static step, (b) smooth step axial load application.
Fig. 19. Failure modes of bare and strengthened columns under combined axial and impact loading.
Fig. 20. Influence of axial compressive loading on the lateral displacements of strengthened and bare steel columns.
Fig. 21. Effect of number of CFRP layers on impact force- lateral displacement response.
Fig. 22. Effect of number of CFRP layers on (a) lateral displacement-time, (b) axial displacement-time response.

List of Figures:

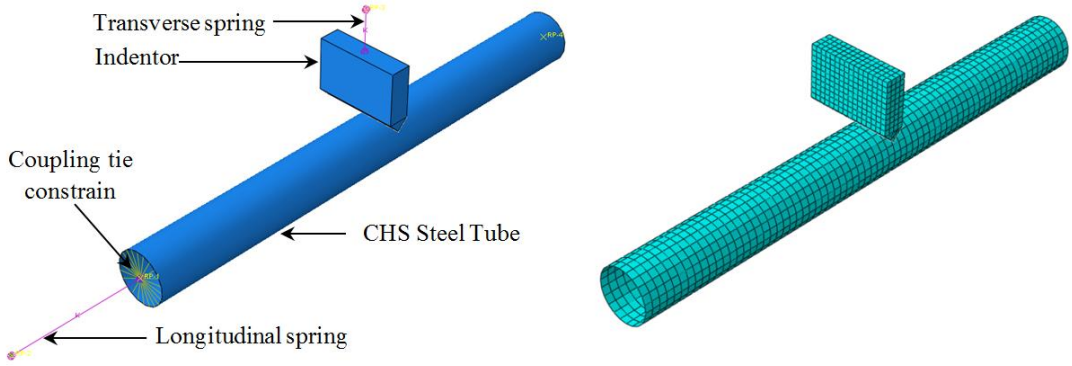

(a) (b)

Fig. 1.

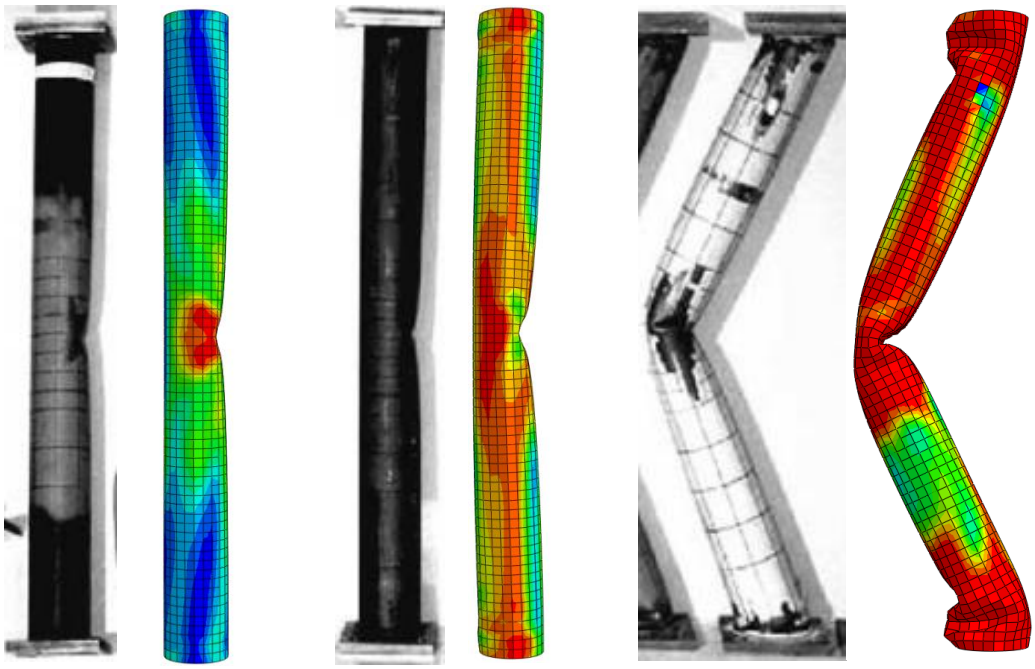

Test FE Test FE Test FE

0% Axial load 50% Axial load 70% Axial load

Fig. 2.

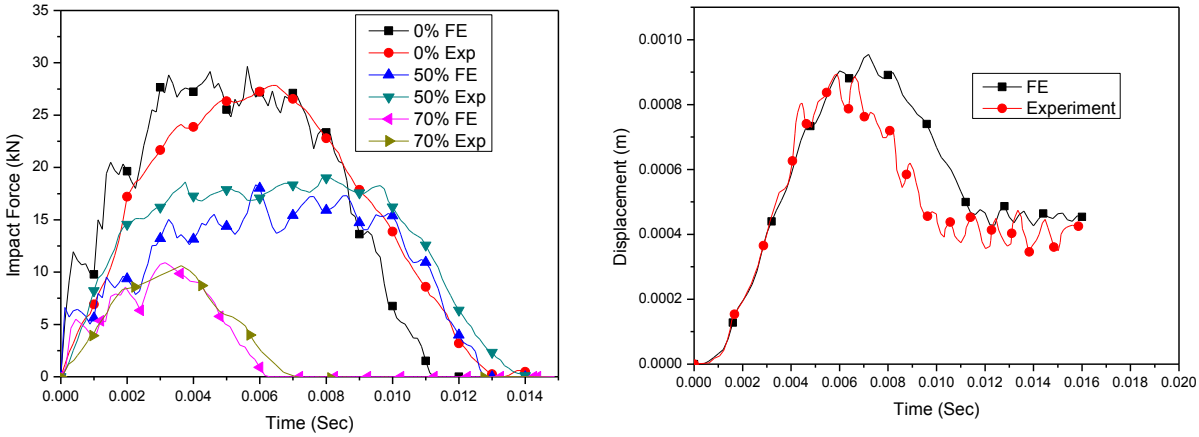
Impact Force (kN)
Time (Sec)
0% FE
0% Exp
50% FE
50% Exp
70% FE
70% Exp
Displacement (m)
Time (Sec)
FE
Experiment

(a) (b)

Fig. 3.

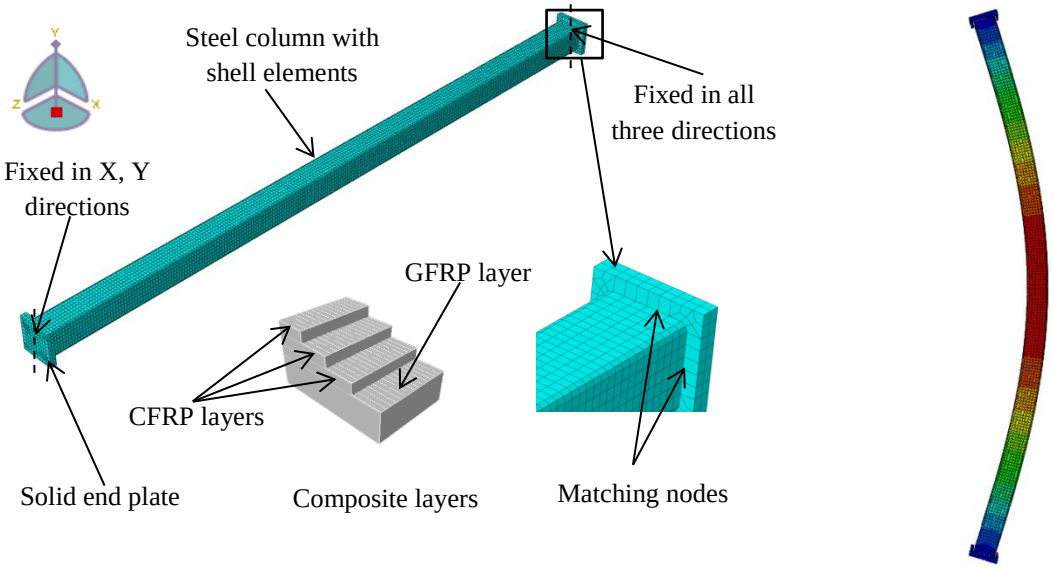
Steel column with
shell elements
Fixed in all
three directions
Fixed in X, Y
directions
GFRP layer
CFRP layers
Solid end plate
Composite layers
Matching nodes

(a) (b)

Fig. 4.

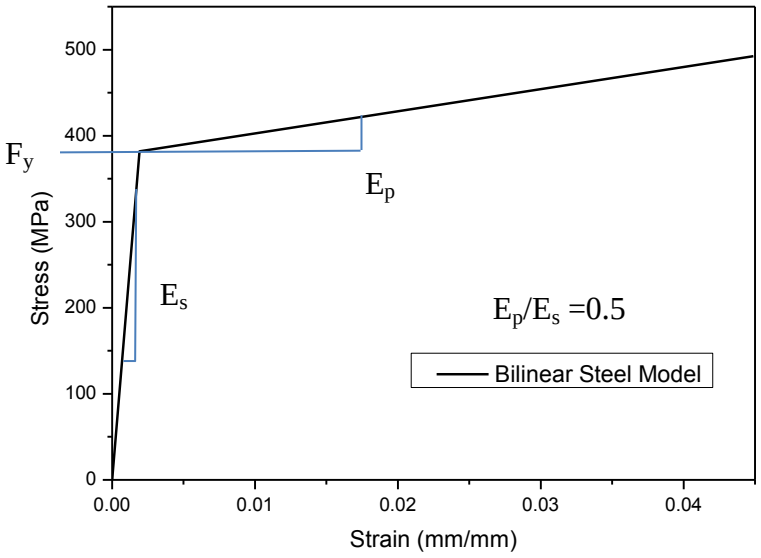
500
400
300
200
100
0
Stress (MPa)
0.00
0.01
0.02
0.03
0.04
Strain (mm/mm)
F_y
E_p
E_s
E_p/E_s =0.5
Bilinear Steel Model

Fig. 5.

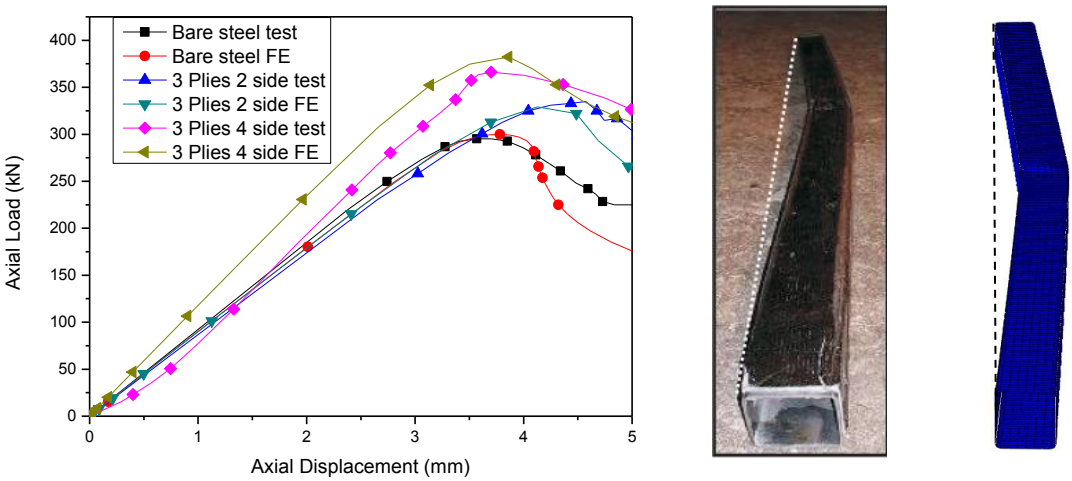
Bare steel test
Bare steel FE
3 Plies 2 side test
3 Plies 2 side FE
3 Plies 4 side test
3 Plies 4 side FE
Axial Load (kN)
Axial Displacement (mm)
0
50
100
150
200
250
300
350
400
0
1
2
3
4
5

(a) (b)

Fig. 6.

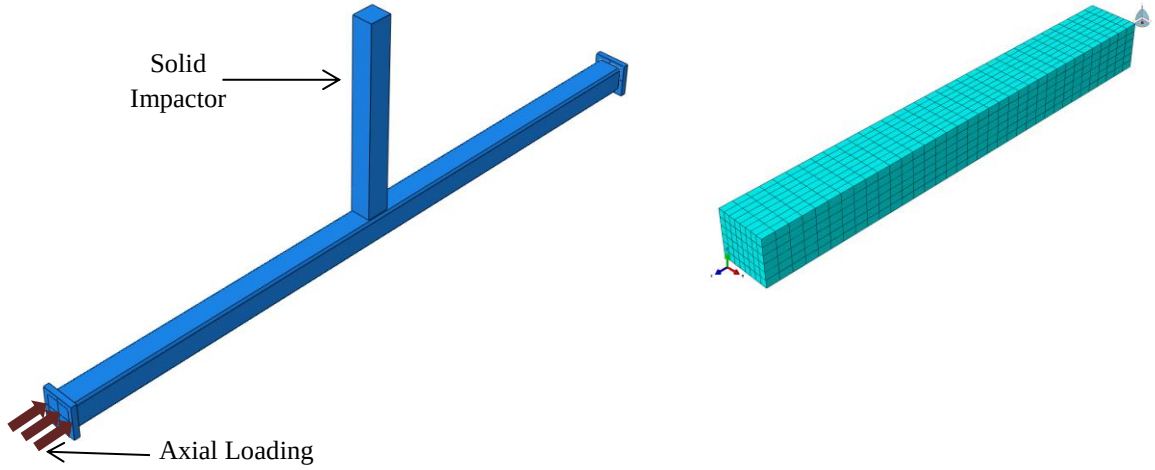

(a) (b)

Fig. 7.

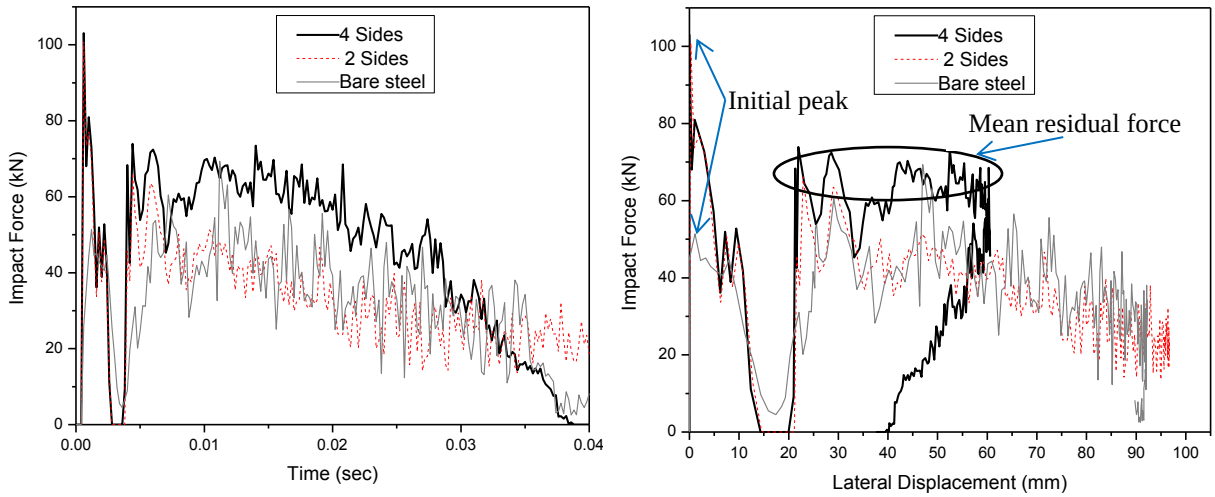
4 Sides
2 Sides
Bare steel
Impact Force (kN)
Time (sec)
Initial peak
Mean residual force
Lateral Displacement (mm)

(a) (b)

Fig. 8.

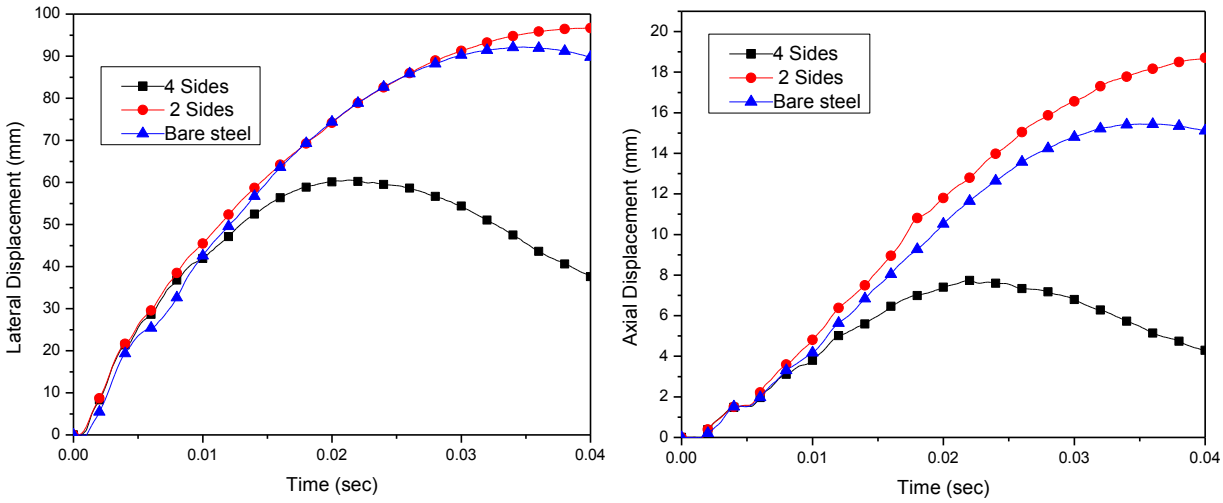
Lateral Displacement (mm)
Time (sec)
4 Sides
2 Sides
Bare steel
Axial Displacement (mm)
Time (sec)
4 Sides
2 Sides
Bare steel

(a) (b)

Fig. 9.

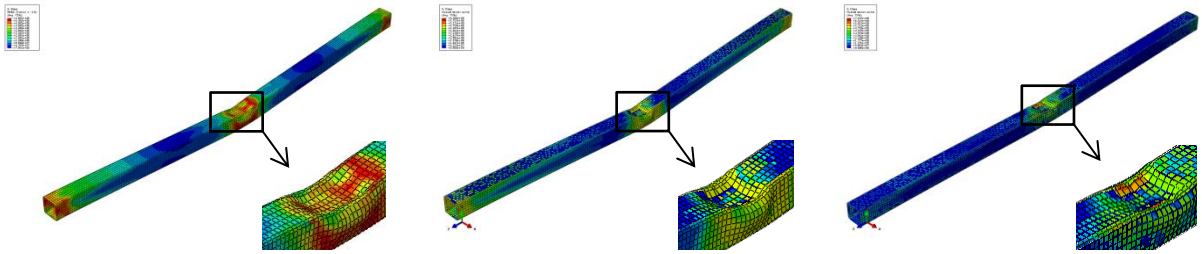

(a) (b) (c)

Fig. 10.

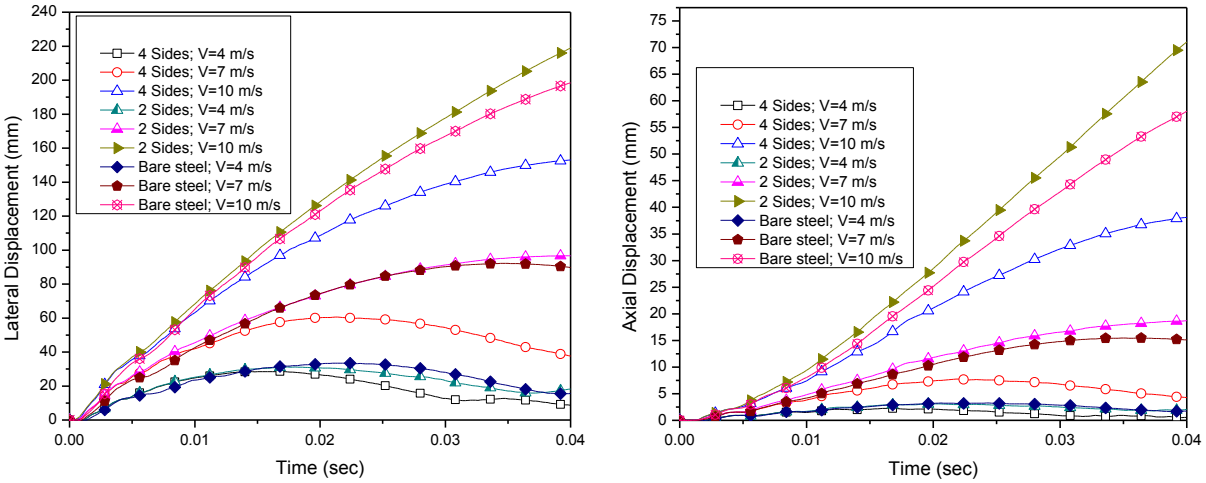
Lateral Displacement (mm)
Time (sec)
4 Sides; V=4 m/s
4 Sides; V=7 m/s
4 Sides; V=10 m/s
2 Sides; V=4 m/s
2 Sides; V=7 m/s
2 Sides; V=10 m/s
Bare steel; V=4 m/s
Bare steel; V=7 m/s
Bare steel; V=10 m/s
Axial Displacement (mm)
Time (sec)
4 Sides; V=4 m/s
4 Sides; V=7 m/s
4 Sides; V=10 m/s
2 Sides; V=4 m/s
2 Sides; V=7 m/s
2 Sides; V=10 m/s
Bare steel; V=4 m/s
Bare steel; V=7 m/s
Bare steel; V=10 m/s

(a) (b)

Fig. 11.

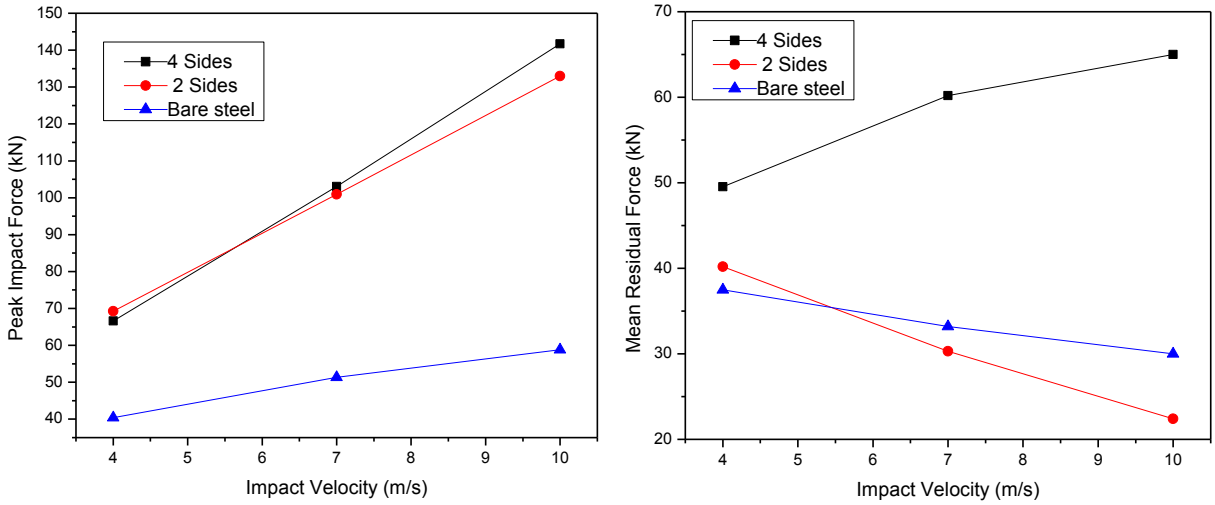
Peak Impact Force (kN)
Impact Velocity (m/s)
4 Sides
2 Sides
Bare steel
Mean Residual Force (kN)
Impact Velocity (m/s)
4 Sides
2 Sides
Bare steel

(a) (b)

Fig.12.

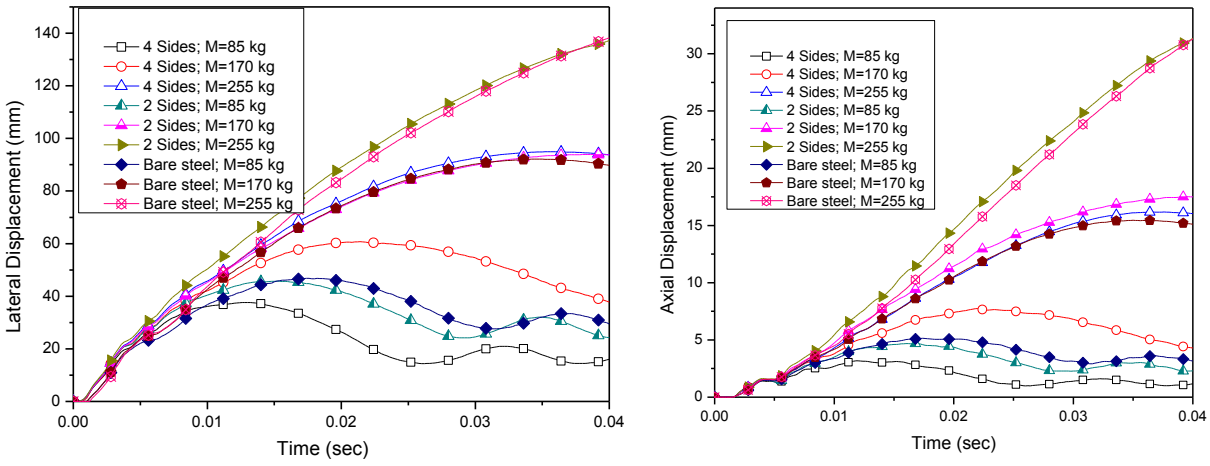
4 Sides; M=85 kg
4 Sides; M=170 kg
4 Sides; M=255 kg
2 Sides; M=85 kg
2 Sides; M=170 kg
2 Sides; M=255 kg
Bare steel; M=85 kg
Bare steel; M=170 kg
Bare steel; M=255 kg
Lateral Displacement (mm)
Axial Displacement (mm)
Time (sec)
0.00
0.01
0.02
0.03
0.04
0
20
40
60
80
100
120
140
5
10
15
20
25
30

(a) (b)

Fig. 13.

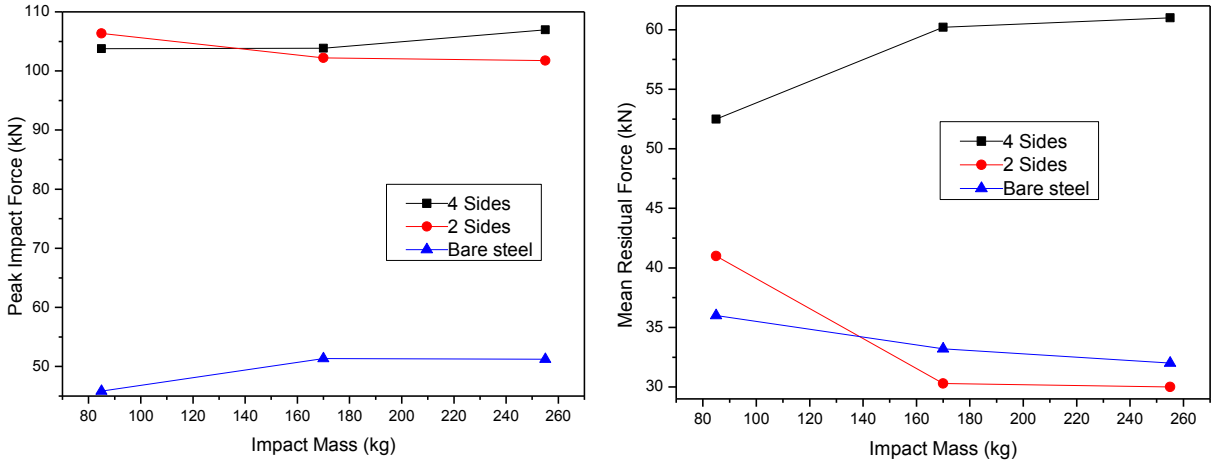
Peak Impact Force (kN)
Impact Mass (kg)
4 Sides
2 Sides
Bare steel
Mean Residual Force (kN)
Impact Mass (kg)
4 Sides
2 Sides
Bare steel

(a) (b)

Fig. 14.

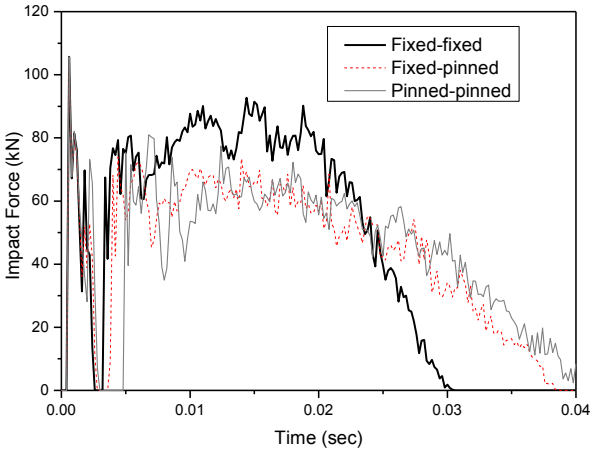
Fixed-fixed
Fixed-pinned
Pinned-pinned
Impact Force (kN)
Time (sec)
0
20
40
60
80
100
120
0.00
0.01
0.02
0.03
0.04

(a)

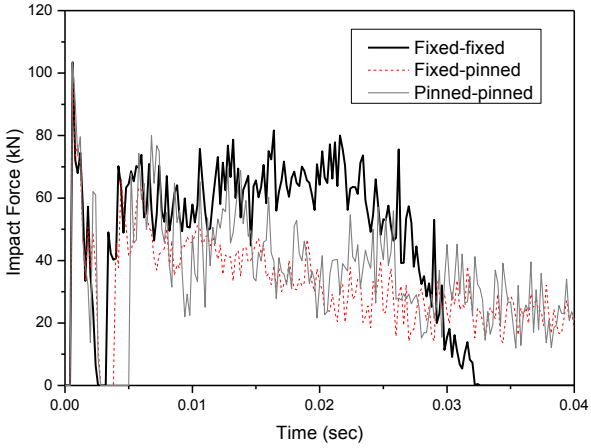
Fixed-fixed
Fixed-pinned
Pinned-pinned
Impact Force (kN)
Time (sec)
0
20
40
60
80
100
120
0.00
0.01
0.02
0.03
0.04

(b)

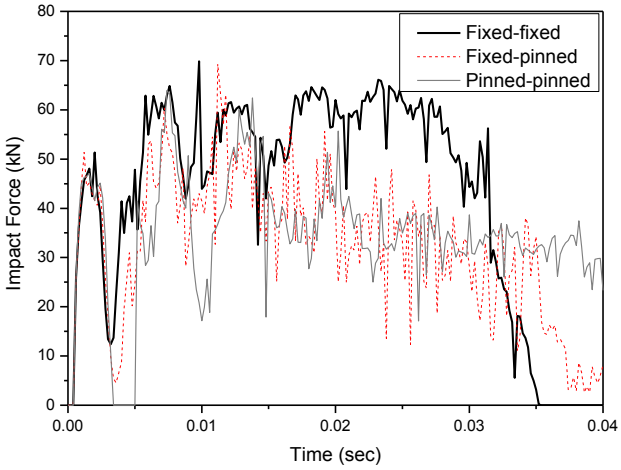
Fixed-fixed
Fixed-pinned
Pinned-pinned
Impact Force (kN)
Time (sec)
0
10
20
30
40
50
60
70
80
0.00
0.01
0.02
0.03
0.04

(c)

Fig. 15.

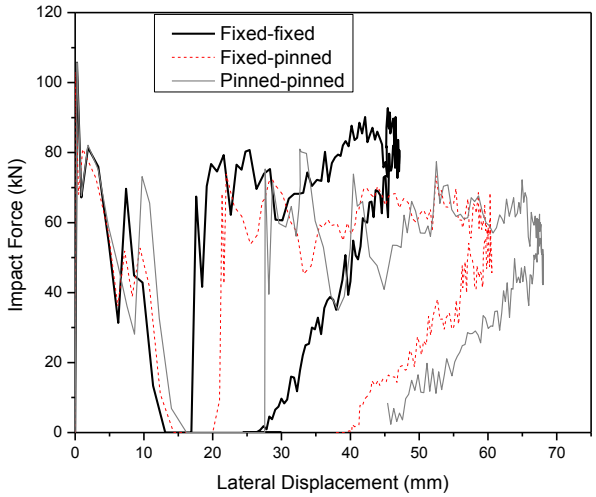
Fixed-fixed
Fixed-pinned
Pinned-pinned
Impact Force (kN)
Lateral Displacement (mm)

(a)

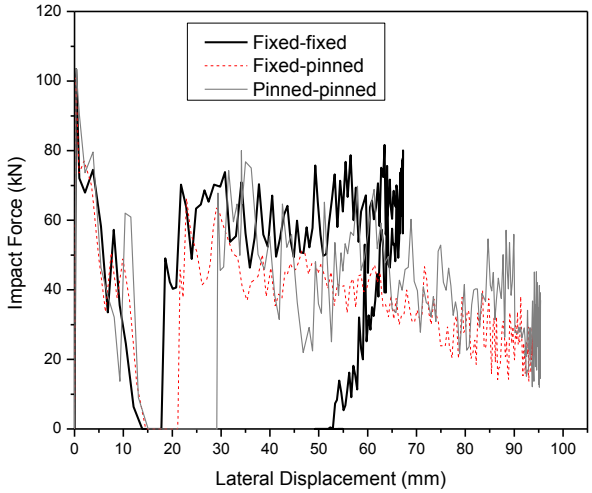
Fixed-fixed
Fixed-pinned
Pinned-pinned
Impact Force (kN)
Lateral Displacement (mm)

(b)

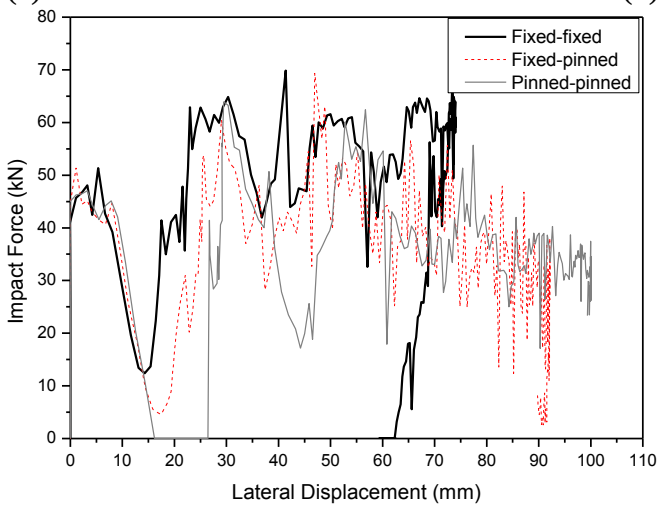
Fixed-fixed
Fixed-pinned
Pinned-pinned
Impact Force (kN)
Lateral Displacement (mm)

(c)

Fig. 16.

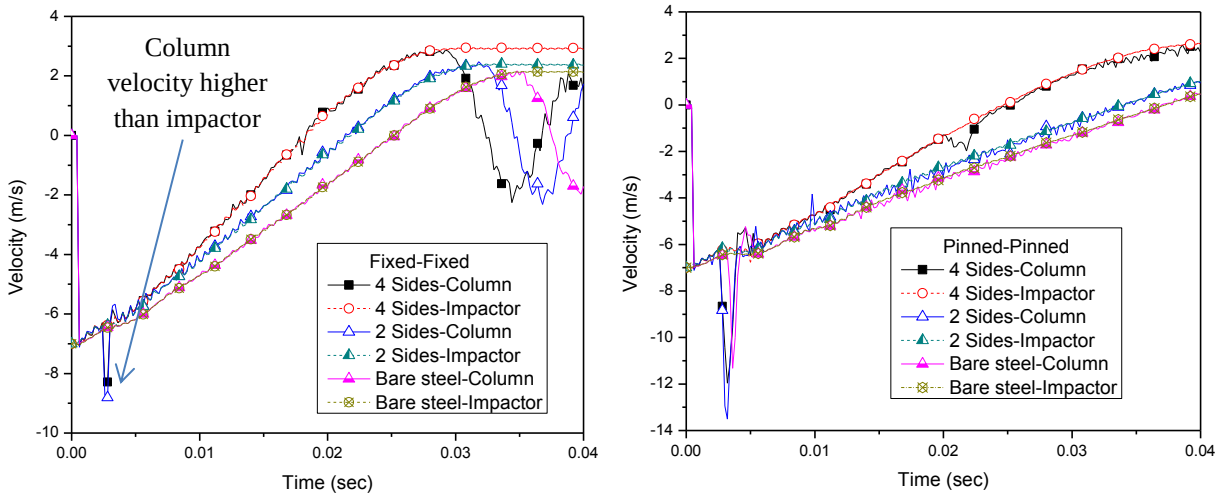
Column
velocity higher
than impactor
Velocity (m/s)
Time (sec)
Fixed-Fixed
4 Sides-Column
4 Sides-Impactor
2 Sides-Column
2 Sides-Impactor
Bare steel-Column
Bare steel-Impactor
Pinned-Pinned
4 Sides-Column
4 Sides-Impactor
2 Sides-Column
2 Sides-Impactor
Bare steel-Column
Bare steel-Impactor

(a) (b)

Fig.17.

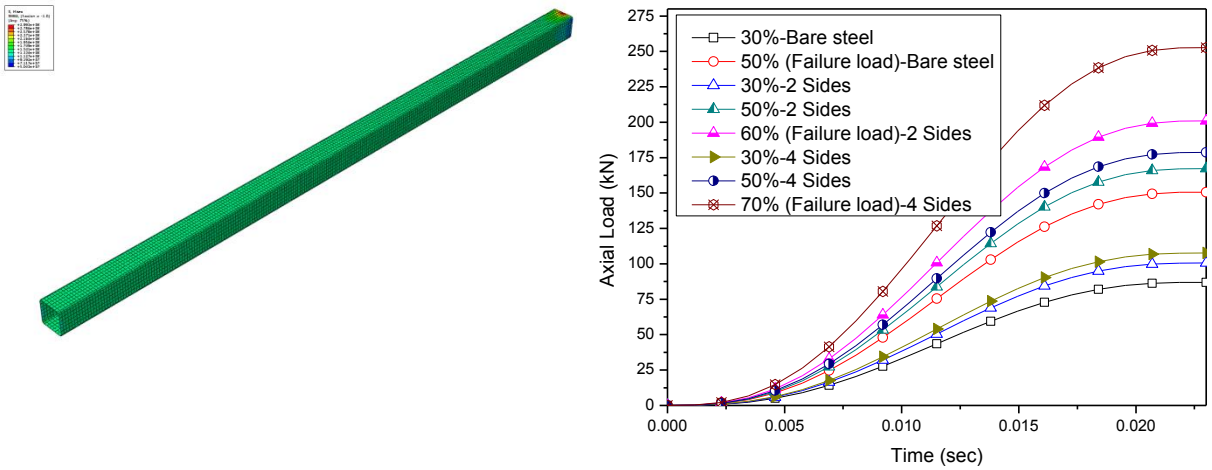
30%-Bare steel
50% (Failure load)-Bare steel
30%-2 Sides
50%-2 Sides
60% (Failure load)-2 Sides
30%-4 Sides
50%-4 Sides
70% (Failure load)-4 Sides
Axial Load (kN)
Time (sec)
0
25
50
75
100
125
150
175
200
225
250
275
0.000
0.005
0.010
0.015
0.020

(a) (b)

Fig. 18.

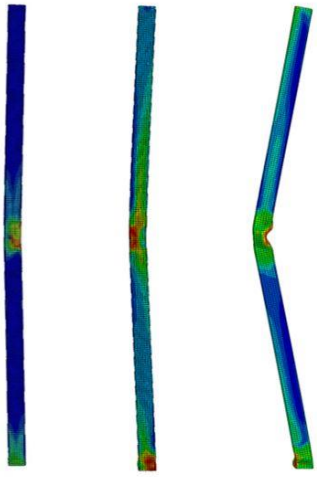

P/ P_{test}=0 P/ P_{test}=0.3 P/P_{test}=0.5

Bare steel

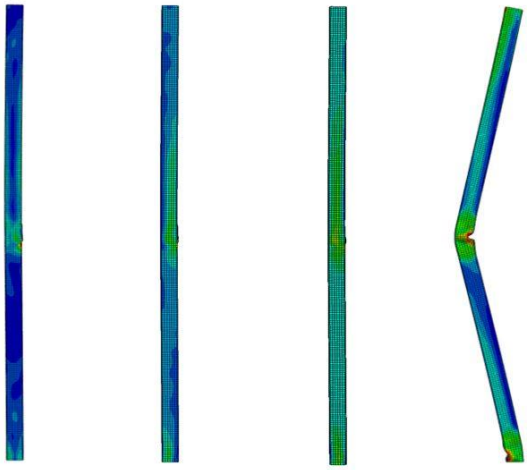

P/ P_{test}=0 P/ P_{test}=0.3 P/ P_{test}=0.5 P/ P_{test}=0.6

2 sides

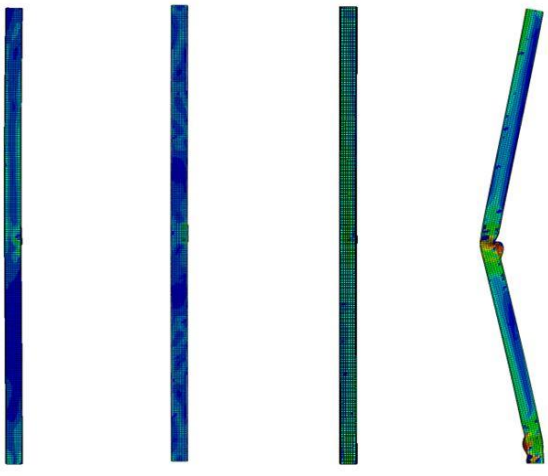

P/ P_{test}=0 P/ P_{test}=0.3 P/ P_{test}=0.5 P/ P_{test}=0.7

4 Sides

Fig. 19.

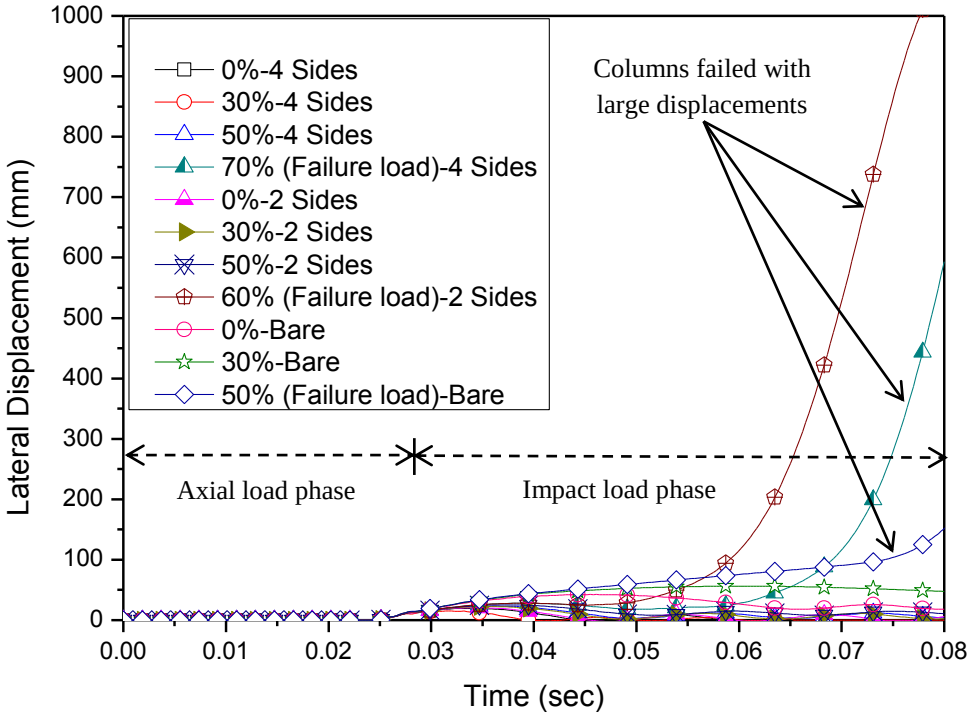
Lateral Displacement (mm)
Time (sec)
0%-4 Sides
30%-4 Sides
50%-4 Sides
70% (Failure load)-4 Sides
0%-2 Sides
30%-2 Sides
50%-2 Sides
60% (Failure load)-2 Sides
0%-Bare
30%-Bare
50% (Failure load)-Bare
Columns failed with large displacements
Axial load phase
Impact load phase

Fig. 20.

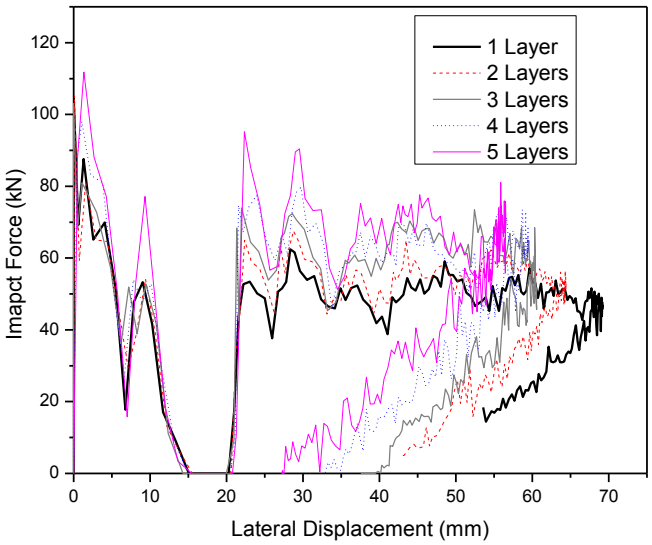
1 Layer
2 Layers
3 Layers
4 Layers
5 Layers
Imapct Force (kN)
Lateral Displacement (mm)
0
20
40
60
80
100
120
0
10
20
30
40
50
60
70

Fig. 21.

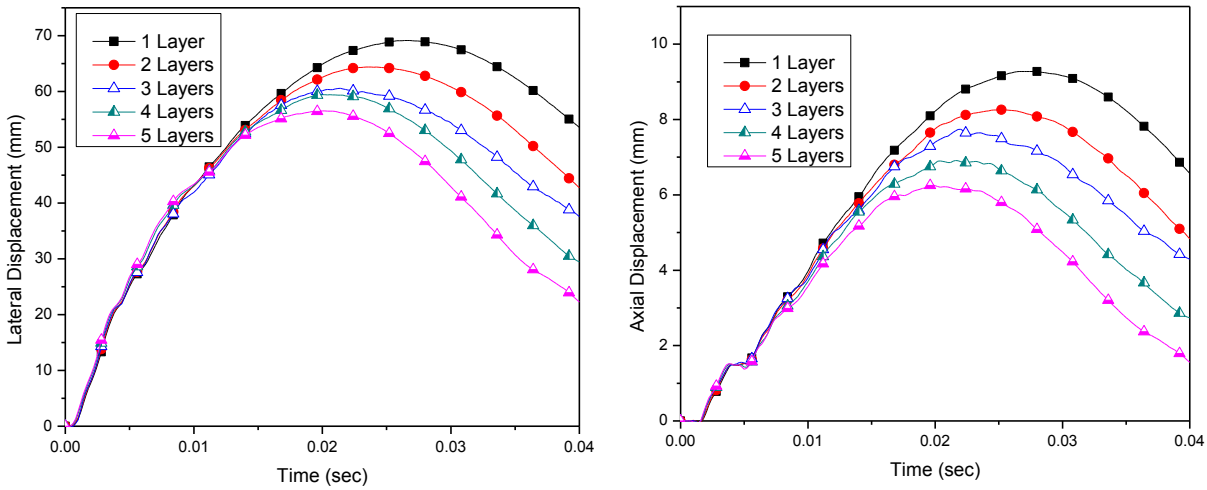
1 Layer
2 Layers
3 Layers
4 Layers
5 Layers
Lateral Displacement (mm)
Time (sec)
0
10
20
30
40
50
60
70
0.00
0.01
0.02
0.03
0.04
1 Layer
2 Layers
3 Layers
4 Layers
5 Layers
Axial Displacement (mm)
Time (sec)
0
2
4
6
8
10
0.00
0.01
0.02
0.03
0.04

(a) (b)

Fig. 22.

List of tables:

Table 1 Material Properties for FE analysis

	Parameters	Value			Parameters	Value
Steel	ρ_s (kg/m^3)	7850		GFRP lamina	ρ_{GFRP} (kg/m^3)	2550
	E_s (GPa)	200			E_{GFRP} (GPa)	17.6
	F_y (MPa)	380			X_{GFRP} (MPa)	336
	ν	0.3			$\varepsilon_{t(GFRP)}$	0.020
CFRP lamina	ρ_{CFRP} (kg/m^3)	2120			$\varepsilon_{c(GFRP)}$	0.012
	E_{CFRP} (GPa)	230				
	X_{CFRP} (MPa)	510				
	$\varepsilon_{t(CFRP)}$	0.0022				
	$\varepsilon_{c(CFRP)}$	0.0013				

Table 2 Comparison between experimental results and present FE analysis

Specimen	Ultimate Load (kN)		Axial shortening at ultimate load (mm)		P_{test} / P_{FE}	U_{Test} / U_{FE}
	Test (P_{test})	FE (P_{FE})	Test (U_{Test})	FE (U_{FE})		
Control	295	299.81	3.70	3.78	0.98	0.98
2 Sides	335	329.08	4.57	4.13	1.02	1.02
4 Sides	362	382.27	3.70	3.86	0.95	0.96
Mean					0.98	0.99
COV					0.036	0.031

Table 3 Summary of axial load application

Column Type	Percentage of failure load (P/ P_{test})	Axial Load (kN)	Stability
Control	30%	88.5	stable
	50%	147.5	failed
	70%	--	--
2 Sides CFRP	30%	100.5	stable
	50%	167.5	stable
	60%	201	failed
4 Sides CFRP	30%	108.6	stable
	50%	181	stable
	70%	253	failed